Exchange of Heat and Flow Between Porous and Non-Porous Region at Different Reynolds Numbers and Permeabilities

EXCHANGE OF FLOW BETWEEN POROUS AND NON-POROUS REGIONS AT DIFFERENT REYNOLDS NUMBERS: LES STUDY

Jadidi M.*, Mahmoudi Y.
*Author for correspondence
Department of Mechanical, Aerospace and Civil Engineering (MACE), University of Manchester, M13 9PL, UK
E-mail: mohammad.jadidi@manchester.ac.uk

ABSTRACT

The physics underlying the exchange of heat and flow between the porous and non-porous regions in a composite porous-fluid system has not been fully understood. In the present paper, a composite porous-fluid system is investigated using pore-scale LES analysis where the complete flow field is resolved in the non-porous region and within the pores of the porous region. We study the effects of the Reynolds number on the flow leakage (flow leakage is the portion of the fluid pushed upwards to the porous-fluid interface due to the negative vertical pressure gradient inside the porous block) from the porous to the non-porous region. To discuss the influences of the Reynolds number on the flow leakage, discussions are made regarding velocity, pressure and temperature fields, coherent structures, and turbulence production. Flow visualization demonstrates the formation of organized counter-rotating vortex pairs (CRVPs) of fluid flow within and above the porous blocks due to the flow leakage. The CRVPs originate from the bottom of the porous block and move upwards altering the coherent structures of the flow above the interface. Moreover, iso-surfaces of vortex strength above the porous interface show a forest of vortices with a clear hairpin structure for all the cases. The distribution of streamlines indicates that the rotation of the legs of the hairpin structures is consistent with the CRVPs above the porous interface. Finally, it is found that all the above discussions about the flow structure and exchange of heat and flow between the porous and non-porous regions can be modified by changing the Reynolds number.

NOMENCLATURE

S_{ij}	Strain rate tensor (1/s)
t	Time (s)
u	Streamwise velocity component (m/s)
U	Velocity at the inlet (m/s)
v	Vertical velocity component (m/s)
x	Streamwise direction
y	Vertical direction
z	Spanwise (Lateral) direction
Symbol	
Δ	Filter width (m)
ε	Porosity (-)
ν	Molecular kinematic viscosity (m/s^2)
$\langle\ \rangle$	Time-averaged value (-)
Subscript	
rms	Root mean square
SGS	Sub-grid scale
Superscript	
$\bar{}$	Filtered

INTRODUCTION

Turbulent flow in porous media is ubiquitous in nature and its understanding is central for unravelling the physics underlying the natural phenomena in food drying, and soil evaporation as well as fostering technological development in engineering applications including packed bed reactors, energy storage, and electronics cooling. In these natural and engineering applications, a step change in the fundamental understanding of flow in porous-fluid systems, which consists of a fluid-saturated porous medium and a flow passing over it is crucial for the characterisation and diagnostic analysis of such complex problems[1].

There have been numerous experimental measurements and numerical simulations of fluid flow in channels fully or partly blocked by a porous medium. Partial blockage of the flow area adds another unknown to the problem: 'the interface modelling of a porous and non-porous region'. Interface modelling remains a challenging question in the literature[2, 3]. While physically one expects much lower fluid velocity in the pores compared to that of free flow, capturing this sharp gradient at the interface can add to the difficulties of the numerical simulation. Beavers and Joseph [4] were amongst the first to show that sharp gradients at the interface between the porous and fluid regions exist. Their work highlighted the existence of a slip velocity at the interface. From there, authors have established different interface conditions that can be classified into two main types according to Alazmi and Vafai [5]: slip and no-slip boundary conditions. Those authors then establish five main categories for the hydrodynamic interface conditions that they critically examined.

Experimental measurements of fluid flow in channels partly blocked by a porous show that there are obvious interactions between the porous region and the non-porous region passing over the porous block. Leu et al. [6] have investigated the flow passing through and over three porous structures with different porosities. Results reveal that above the porous structure there are complex interactions between the flow within the porous and the flow passing above the porous structure. Results show that as the structure porosity increases, the flow velocity, turbulence intensity and Reynolds shear stress all decrease. Suga et al. [7] also have used PIV to conduct an extensive investigation on the effect of the permeability and Reynolds number on the flow over a permeable layer. Findings show that the normal-wall Reynolds stress is enhanced by an increase in the permeability of the permeable wall or bulk Reynolds number. This tendency is not seen in the streamwise component. This enhancement of the wall-normal stress near the permeable layer is attributed to the weakening of the blocking effect of the permeable boundary,

which in turn contributes to a higher level of Reynolds shear stress at the interface.

In the present study, the flow features for a channel partially filled with three Re numbers are investigated numerically using a detailed pore-scale large eddy simulation (LES) approach. LES approach is a high fidelity turbulence modelling that captures both laminar and turbulent flow behaviours that occur in this study. Therefore LES is utilized in the present study. The effect of the porous block on the coherent structures and the large reverse flow pattern along the top surface of the block is investigated. Moreover, the effect of the flow leakage from the porous region to the non-porous region on coherent structures is examined in detail.

COMPUTATIONAL DOMAIN & BOUNDARY CONDITION

The computational domain is a channel partially filled with a porous block depicted in Figure 1. The porous block is formed from a rectangular cross-section ligament with a thickness of 0.26D where D is the consecutive distance between two ligaments. The blockage ratio (i.e., the ratio of the height of the porous region to the channel height) is 0.5 in all cases which is a typical value that is utilized for fundamental studies such as the present paper[8, 9]. The computational domain has the dimensions of 70D, 6D, and 5D in the x, y, and z directions, respectively. The flow Reynolds numbers (based on the channel hydraulic diameter) are 3600, 7200 and 14400.

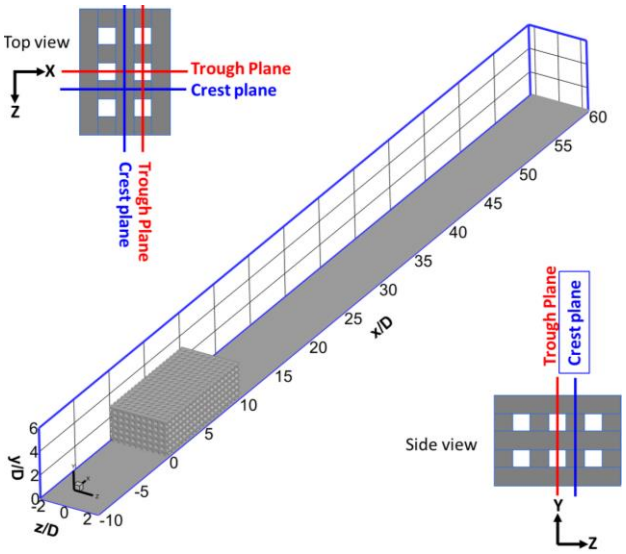

Figure 1 Computational domain; Porous block formed from rectangular cross-section ligament (porosity 46.4%); The blue line lies over the crest plane and the red line lies over the trough plane

NUMERICAL METHOD

The LES filtered equations are acquired as in Eqs. (1) – (2):

$$\frac{\partial \overline{u_i}}{\partial x_i} = 0 \qquad (1)$$

$$\frac{\partial \overline{u_i}}{\partial t} + \frac{\partial}{\partial x_j}(\overline{u_i u_j}) = -\frac{1}{\rho}\frac{\partial \overline{p}}{\partial x_i} + \frac{\partial}{\partial x_j}\left((\nu + \nu_{SGS})\frac{\partial \overline{u_i}}{\partial x_j}\right) \qquad (2)$$

where, $\overline{u_i}$, and $\overline{p}$ are the filtered velocity in ith direction, the and pressure respectively [12]. The filter function is taken as a simple box filter, Δ, with filter width equal to the cube root of cell volume. In the present study, the ν_{SGS} is modelled using the dynamic SGS turbulent kinetic energy model Davidson [10].
The filtered governing equations are discretized by implementing the finite volume method. All the computations are carried out in the open-source object-oriented C++ programming in the OpenFOAM CFD package[11]. The second order central difference scheme is adopted for spatial discretization. The implicit second-order backward difference scheme is used for the time integration. The PISO is taken on for the pressure–velocity coupling in all the present simulations[12]. To accurately capture the evolution of the flow features, the physical time step is chosen for each grid such that the CFL number is kept below unity. This is true for the most refined portions of each grid enforcing a constant time step of $\Delta t = 1\times10^{-5}\ s$. Time averaging process is begun when the initial transient conditions are washed out and a semi-steady state operating condition is reached. All the present numerical results are averaged over a period of 490 non-dimensional time units ($t^* = t \times U/D$), where U is the flow mean velocity at the channel inlet. The computational domain is discretized into 10.3 million non-uniform cells with a minimum grid spacing of 0.01D in the x, y, and z directions. The grid resolution is assessed based on the two-point correlation that has been implemented by [13]. it is found that at least 6 cells have been included in the vertical integral length scale seeming to be sufficient [14].

VALIDATION OF NUMERICAL MODELS

The developed LES solver has been validated with respect to the experiment [6]. compares the present LES results and experimental data for streamwise and vertical velocity components, Reynolds shear stress and turbulent kinetic energy above the porous block in the wake region at $X/H = 3$. The figure shows that the developed LES model can predict well the experimental data at locations above the porous block and in the wake downstream of the porous block.

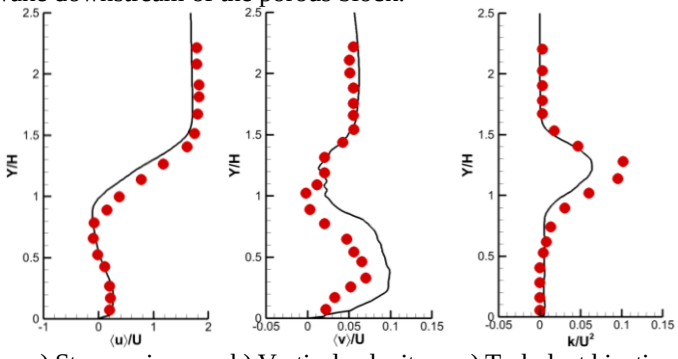

a) Streamwise velocity b) Vertical velocity c) Turbulent kinetic energy

Figure 2 Comparison of velocity profiles and turbulent kinetic energy TKE $= 0.5\left(\overline{u'^2} + \overline{v'^2} + \overline{w'^2}\right)$ obtained from the present LES study (solid lines), against the experimental measurements (symbols) [6]

RESULTS AND DISCUSSION

Contours of time-averaged streamwise velocity on the trough plane (see Figure 1) for the three Re numbers are presented in Figure 3. It is seen that the velocity fields are similar for the three cases. As it can be seen the porous media allow the flow to penetrate the void spaces (pores) of the porous block. Consequently, the velocity magnitude is reduced in the clear region above the porous block, and the reverse flow pattern on the top surface of the porous block usually observed for the solid block has deteriorated. The figures show that for all cases, there exists a recirculation region downstream of the blocks.

Vertical distributions of time-averaged streamwise velocity through and above the porous region for Re=3600 are shown in **Figure 4**. As revealed in **Figure 4** the velocity profiles have a non-uniform wavy shape within the porous block due to the geometrical characteristics of the pores. Besides, the streamwise velocity within the porous regions experiences an acceleration and deceleration continuously due to contractions and expansions of the flow as it passes through the pores.

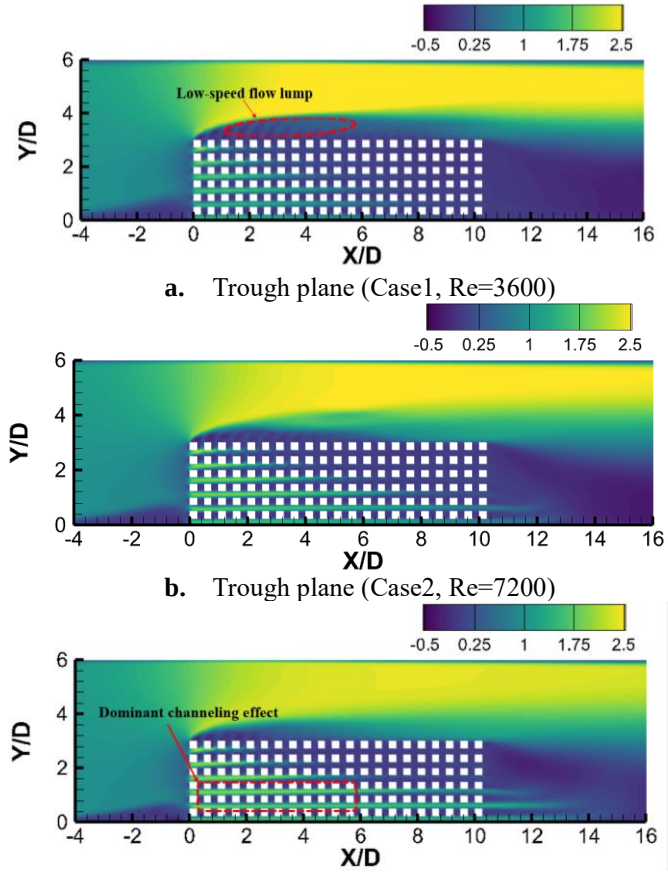

a. Trough plane (Case1, Re=3600)

b. Trough plane (Case2, Re=7200)

c. Trough plane (Case3, Re=14400)

Figure 3 Contours of time-averaged streamwise velocity on the trough plane for three Re numbers (front view)

The figures also show an important channeling effect when the flow passes through the gap between the ligaments and the bottom wall. Mean velocity profiles at various streamwise locations in **Figure 4** demonstrates that as the flow moves downstream, the velocities within the porous region are retarded by the presence of the porous medium and flow leakage from the porous block to the non-porous region. The results are consistent with the contours of streamwise velocity on the trough plane for the porous block discussed in Figure 3.

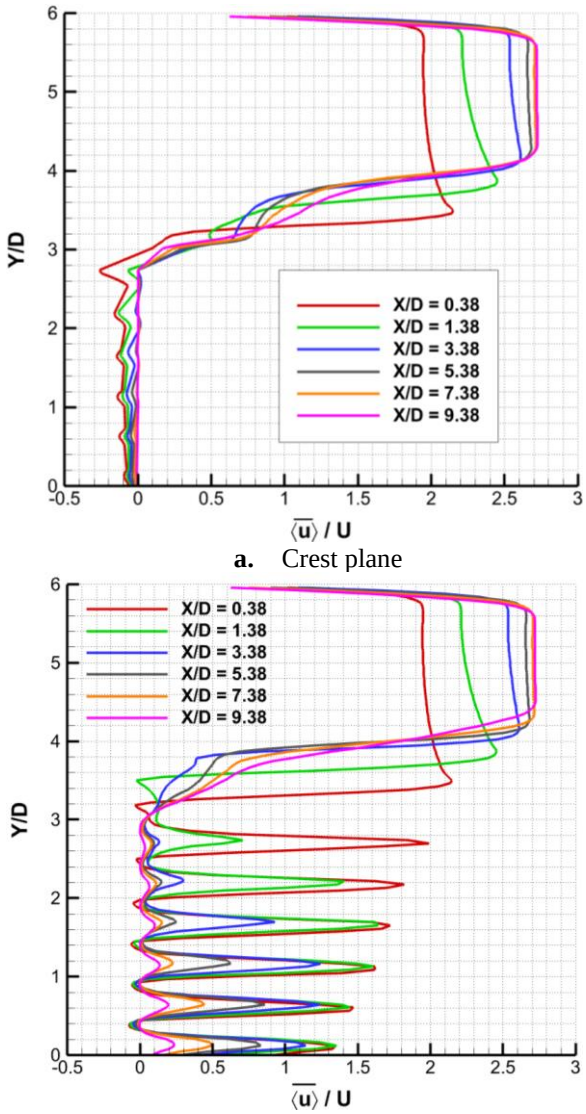

a. Crest plane

b. Trough plane

Figure 4 Vertical distributions of non-dimensional time-averaged streamwise at Re=3600

Figure 5 shows the contours of time-averaged vertical velocity. The very first visible feature is that some portion of the fluid entering the porous blocks is pushed upwards toward the porous-fluid interface and leaves the porous region halfway through to the clear region (positive leakage). This phenomenon is represented by the horizontal distributions of time-averaged vertical velocity on the interface region for three cases with different Re numbers in Figure 6. Figure 6 displays the horizontal distribution of the time-averaged vertical velocities on the interface for the three cases. The vertical velocity lessens by moving downstream along the interface; meaning that the flow leakage decreases from the leading edge toward the downstream. Also, as illustrated in Figure 5, flow leakage reduces as Re rises

which is quantified clearly in Figure 6. A comparison of vertical velocities at different streamwise locations (x/D) implies that the lower Re number possesses a higher vertical velocity and consequently a higher flow leakage.

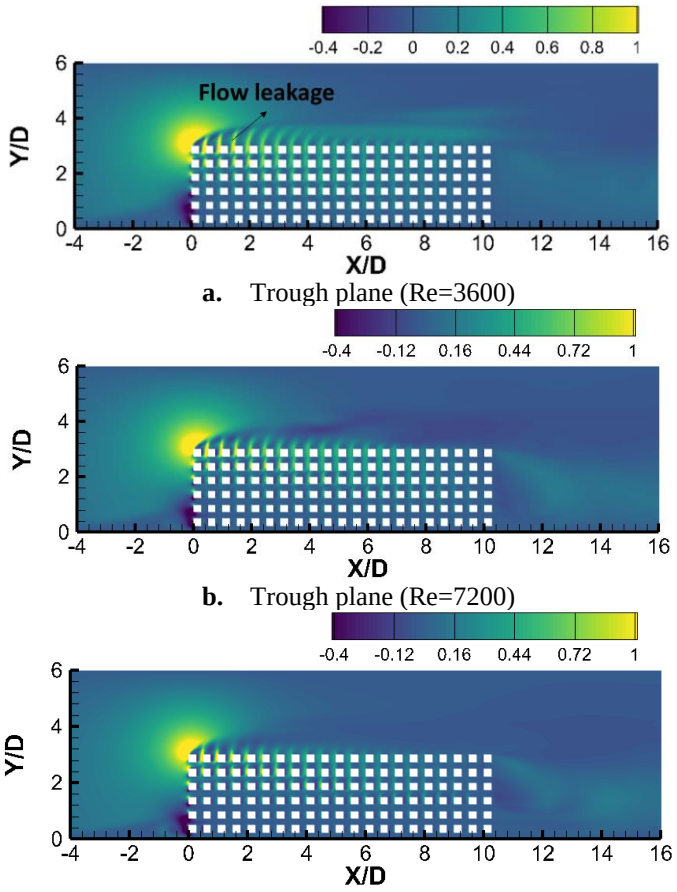

Figure 5 Contours of time-averaged vertical velocity for three Re numbers

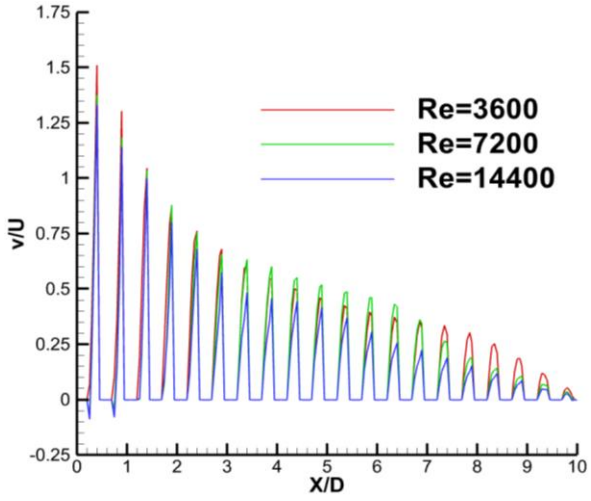

Figure 6 Horizontal distributions of time-averaged vertical velocity on the interface region for three cases with different Re numbers

To accurately compare the flow leakage for three Re numbers, Table 1 presents the absolute and relative flow rates that drip from the porous block into the non-porous region up to streamwise locations $X/D = 2.5, 5, 7.5$. Q_{in} illustrates the time-averaged flow rate that enters the porous block from the windward face and Q_{lx} is the time-averaged flow rate that leaks from the X-percentage of the interface surface. Table 1 indicates that the higher the Re number, the larger the flow rate entering the porous block (Q_{in}). In addition, more than 60% of the flow entering the porous blocks exits from the porous interface before $X/D = 7.5$ for three Re numbers; this even intensifies when the Re number decreases (84% for Re=3600). Finally, relative flow rates (Q_{lX}/Q_{in}) at each streamwise section in Table 2 support the discussions of Figures 5 and 6 demonstrating that increasing the Re number reduces the flow leakage (Q_{lx}). Finally, relative flow rates (Q_{lX}/Q_{in}) at each streamwise section in Table 2 support the discussions of Figures 5 and 6 demonstrating that increasing the Re number reduces the flow leakage (Q_{lx}).

Table 1 Absolute and relative values of flow rate that leaks from the porous blocks at different Re numbers

		Re=3600	Re=7200	Re=14400
$Q_{in} \times 10^4$		1.54	3.51	7.42
$Q_{lX}/Q_{in} \times 100$	$X = 2.5$D	44	36	33
$Q_{lX}/Q_{in} \times 100$	$X = 5.0$D	68	59	52
$Q_{lX}/Q_{in} \times 100$	$X = 7.5$D	84	72	62

Side views of the positive leakage from the porous blocks are shown by streamlines in **Figure 7**. The figure demonstrates the upwards tendency of the flow that passes through the porous gap and bleeds into the clear region. Moreover, counter-rotating vortex pairs (CRVPs) of fluid flow within and above the porous blocks are evident from the side view representation of the flow field in **Figure 7**. The figure clearly shows that the CRVPs originate from the bottom of the porous block and move upwards in the y-direction. It is worthwhile to notice that the extent of the CRVPs inside the porous region is constrained by the size of the pores; however, above the interface, their sizes are larger and almost comparable with the size of the ligaments.

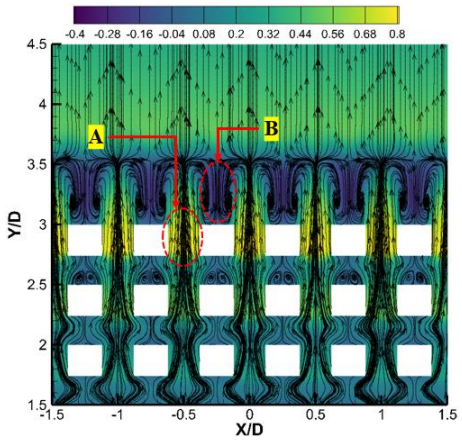

a. Vertical velocity (Re=3600)

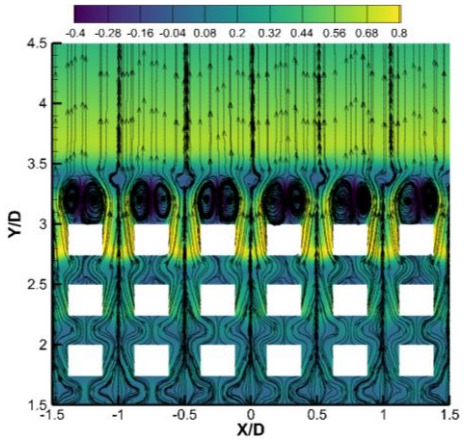

b. Vertical velocity (Re=3600)

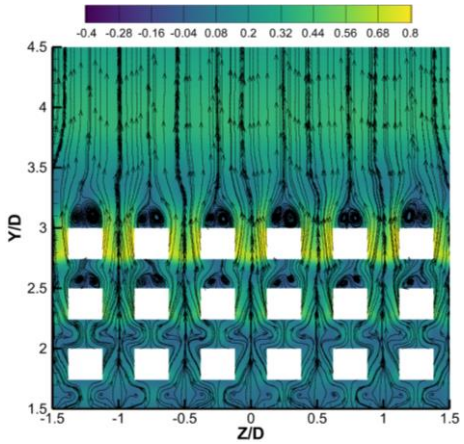

c. Vertical velocity (Re=14400)

Figure 7 Side view contours of time-averaged vertical velocity components, and streamlines on trough planes at x/D=2; **Top**: Re=3600, **Middle**: Re=7200, and **Bottom**: Re=14400

Figure 8 shows iso-surfaces of vortex strength that exhibit a forest of vortices with clear hairpin structure: a spanwise-oriented 'head' connected to counter-rotating quasi-streamwise 'legs. The flow patterns over the porous blocks are almost like those in impermeable wall boundary layers reported by Adrian et al. [18]. As they discussed, the vortex head in Figure 8 corresponds to a hairpin vortex signature aligned in the streamwise direction. However, for the first case with Re=3600 in Figure 8 (a), the hairpin structures are well-organised as it cannot be noticed for the higher Re numbers (Figure 8 (b-c)); it is nearly difficult to visually detect distinctive flow patterns of vortex heads. Figure 8 (b-c) demonstrates the sense of rotation of the legs of the hairpin structures that is consistent with the positive and negative streamwise vorticity above the porous interface demonstrated in **Figure 7**.

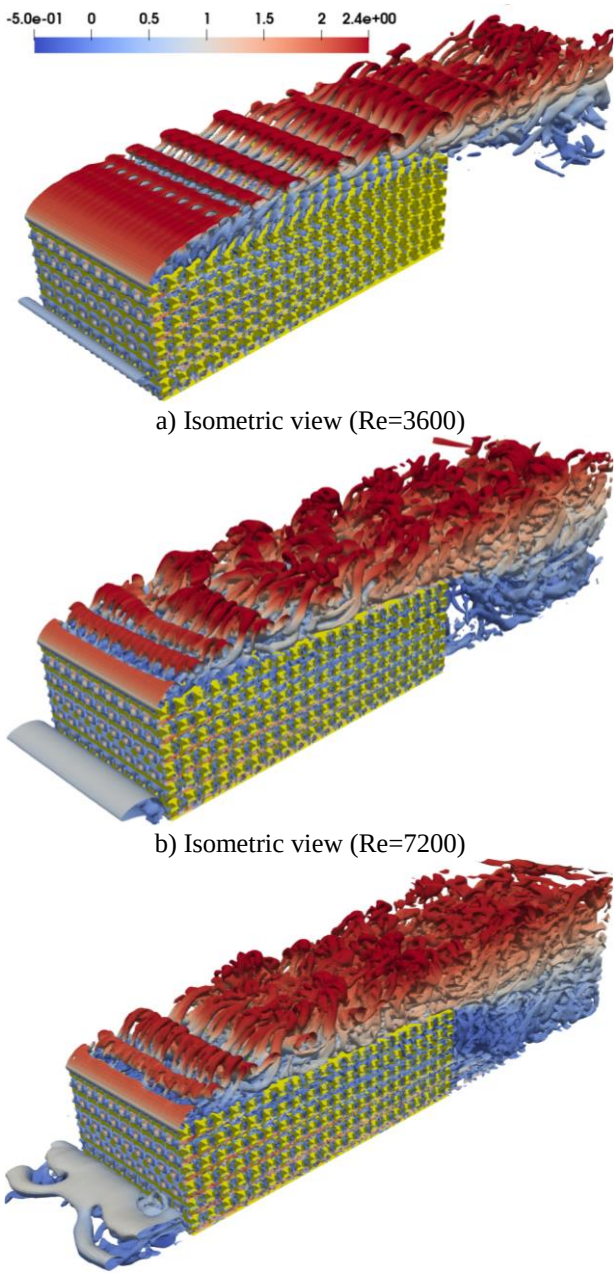

a) Isometric view (Re=3600)

b) Isometric view (Re=7200)

c) Isometric view (Re=14400)

Figure 8 Three-dimensional hairpin coherent structures identified by instantaneous iso-surface of Q-criterion coloured by time-averaged streamwise vorticity

Iso-surface of pressure and vertical velocity fluctuations are depicted for three Re numbers in Figure 9. The fluctuations for Re=3600 indicate that no turbulence exists at the leading edge up to approximately x/D=4.6. This region is characterized by the hairpin vortices as shown in Figure 8. At nearly x/D=4.6, the turbulence production initiates leading to the sudden growth of fluctuations as observable in Figure 9(a-b). The sudden rise of turbulence production at this point for Re=3600 coincides with the emergence of Kelvin-Helmholtz instability vortices as can be seen in Figure 8(a). The Kelvin-Helmholtz instabilities vortices

then roll up along the shear layer above the interface plane and develop downstream as their evolutionary pathways can be perceived in Figure 9 by region with relatively higher values of turbulent fluctuations. At higher Re numbers, the sudden rise of turbulence fluctuations occurs just after the leading edge as shown in Figure 9(c-f). This confirms the formation of Kelvin-Helmholtz instability vortices just at the leading edge for higher Re numbers.

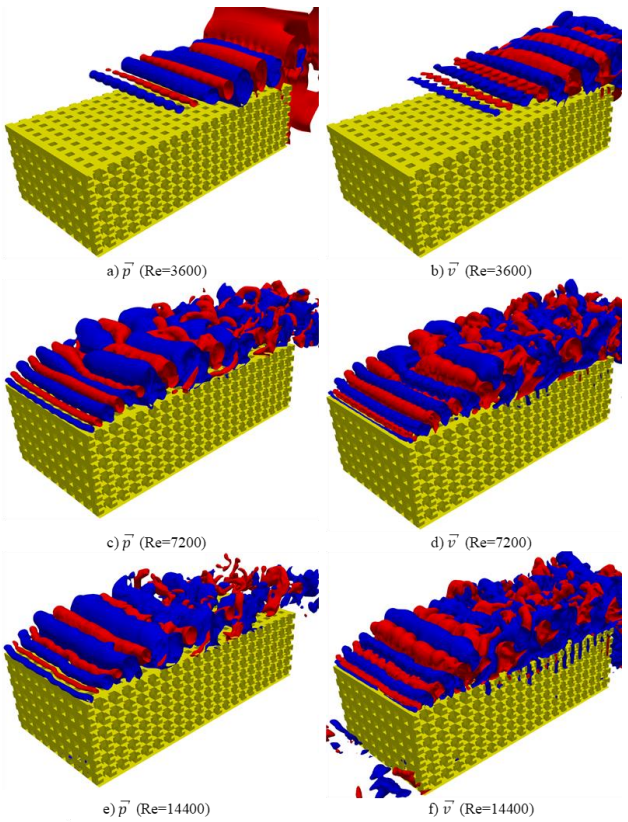

Figure 9 Iso-surface of pressure and vertical velocity fluctuations for three Re numbers

CONCLUSION

Pore-scale LES investigation has been conducted to better understand the flow features of a channel partially filled with a porous block. Results show that the boundary layer at the porous-fluid interface is continuously disrupted by the positive leakage across the interface. It is also explained that positive leakage has a noticeable effect on the flow separation and reverse flow at the upstream edge of the porous block, coherent structures, and turbulent intensity above the porous-fluid interface. Moreover, LES results indicate that more than 60% of the flow entering the porous blocks exits from the porous interface before $X/D = 7.5$ for three Re numbers; this even intensifies when the Re number decreases (84% for Re=3600).

REFERENCES

[1] Y. Mahmoudi, K. Hooman, and K. Vafai, *Convective heat transfer in porous media*. CRC Press, 2019.

[2] D. A. Nield and A. V. Kuznetsov, "An Historical and Topical Note on Convection in Porous Media," *Journal of Heat Transfer*, vol. 135, no. 6, 2013, doi: 10.1115/1.4023567.

[3] K. Suga and Y. Kuwata, "Turbulence over/inside porous surfaces and challenges to its modelling," *Journal of Physics: Conference Series*, vol. 530, no. 1, p. 12004, 2014, doi: 10.1088/1742-6596/530/1/012004.

[4] G. S. Beavers and D. D. Joseph, "Boundary conditions at a naturally permeable wall," *Journal of Fluid Mechanics*, vol. 30, no. 1, pp. 197-207, 1967, doi: 10.1017/S0022112067001375.

[5] B. Alazmi and K. Vafai, "Constant wall heat flux boundary conditions in porous media under local thermal non-equilibrium conditions," *International Journal of Heat and Mass Transfer*, vol. 45, no. 15, pp. 3071-3087, 2002.

[6] J. M. Leu, H. C. Chan, and M. S. Chu, "Comparison of turbulent flow over solid and porous structures mounted on the bottom of a rectangular channel," *Flow Measurement and Instrumentation*, vol. 19, no. 6, pp. 331-337, 2008/12/01/ 2008, doi: 10.1016/j.flowmeasinst.2008.05.001.

[7] K. Suga, Y. Matsumura, Y. Ashitaka, S. Tominaga, and M. Kaneda, "Effects of wall permeability on turbulence," *International Journal of Heat and Fluid Flow*, vol. 31, no. 6, pp. 974-984, 2010/12/01/ 2010, doi: 10.1016/j.ijheatfluidflow.2010.02.023.

[8] T. Kim, G. Blois, J. L. Best, and K. T. Christensen, "Experimental study of turbulent flow over and within cubically packed walls of spheres: Effects of topography, permeability and wall thickness," *International Journal of Heat and Fluid Flow*, vol. 73, pp. 16-29, 2018-10-01 2018, doi: 10.1016/j.ijheatfluidflow.2018.06.004.

[9] W. P. Breugem, B. J. Boersma, and R. E. Uittenbogaard, "The laminar boundary layer over a permeable wall," *Transport in Porous Media*, vol. 59, no. 3, pp. 267-300, 2005, doi: 10.1007/s11242-004-2557-1.

[10] L. Davidson, *Fluid mechanics, turbulent flow and turbulence modeling*, Chalmers University of Technology, 2021. [Online]. Available: http://www.tfd.chalmers.se/~lada.

[11] "OpenFOAM v2006." www.openfoam.com (accessed.

[12] H. K. Versteeg and W. Malalasekera, *An Introduction to Computational Fluid Dynamics: the Finite Volume Method*, 2nd ed. Harlow, England;: Pearson Education Limited., 2007.

[13] F. Bazdidi-Tehrani, A. Ghafouri, and M. Jadidi, "Grid resolution assessment in large eddy simulation of dispersion around an isolated cubic building," *Journal of Wind Engineering and Industrial Aerodynamics*, vol. 121, pp. 1-15, 2013/10/01/ 2013, doi: https://doi.org/10.1016/j.jweia.2013.07.003.

[14] L. Davidson, "How to estimate the resolution of an LES of recirculating flow," in *Quality and Reliability of Large-Eddy Simulations II*: Springer Netherlands, 2011, pp. 269-286.